Integrated Geological, Fluid Flow and Geomechanical Model of a Geothermal Field

Giovanni Sosio[1], Ann-Sophie Boivineau[1], Oleksandr Burachok[1], Rabah Ould Braham[1], Elodie Zordan[1], Andreia Mandiuc[1], Charidimos Spyrou[1], Mounir Belouahchia[1], Clement Baujard[2], Eleonore Dalmais[2], Albert Genter[2]

[1] Schlumberger, 1 Cours du Triangle, Le Palatin 1, 92936 La Defense, France

[2] ES Géothermie, 3A chemin du gaz, F-67500 Haguenau, France

gsosio@slb.com

Keywords: Geothermal energy, geomechanics, fluid flow, deformation, coupled simulation, fractures.

ABSTRACT

Geothermal reservoirs are often faulted and fractured formations. Highly conductive fractures are the main flow channels and therefore are the primary targets for well placement. During reservoir development, reinjection of cold water at high rates will not only change the stress field but could also reactivate the faults, potentially leading to seismic events. Coupling fluid flow and geomechanical simulators allows the assessment of the possible impact of production-injection activity on the subsurface system, notably the change of flow direction and the closure and opening of fracture networks, affecting the performance of the system as a heat exchanger, and the occurrence of microseismic events due to the reactivation of faults, impacting public acceptance.

This project demonstrates the construction of a coupled reservoir geomechanical model of the Rittershoffen geothermal site located in Northern Alsace (France). The simulation of the impact of future operations in terms of fracture closure and opening and microseismic events is ongoing and will be published subsequently.

1. INTRODUCTION

In the framework of the ECOGI project (Baujard et al 2015), aiming at the construction and operation of the Rittershoffen geothermal plant, eastern France, an integrated geological, fluid flow and geomechanical model has been built.

The Rittershoffen field is located in the Upper Rhine Graben close to the Soultz geothermal anomaly. The shallow sedjmentary layers (0 to 1500 m – 2000 m depth), overlie the crystalline basement, consisting of altered and fractured granitic rocks (Baujard et al 2015). Both formations are crossed by large N-S trending normal faults corresponding to the extension regime of the Rhine graben.

The ECOGI project consists of a geothermal doublet, producing heat which is delivered to an industrial site 15 km from the well site. The two wells were drilled from the same location in 2012 (GRT-1, with vertical depth of 2550 m and measured depth of 2850 m) and 2014 (GRT-2, with vertical depth of 2750 m and measured depth of 3196 m). The target geothermal aquifer, which corresponds to local normal fault called fracture zones (Genter et al., 2015), spans the bottommost sedimentary layers (Buntsandstein) and the top of the granite. The two wells are located approximately 1 km away at the target depth.

2. WELLBORE DATA ANALYSIS

The extent and quality of all the wellbore data from the GRT-1 and GRT-2 wells have been audited, including wireline logs, mud logs, stratigraphy, well sketch and trajectory. The data have been prepared for further analysis and interpretation. The interpretation of wellbore data consisted of three main tasks.

2.1 Petrophysical interpretation

Logs from the two wells were interpreted with a simultaneous equation solver, which inverts the wireline log results at each depth to define the petrophysical and lithological properties (porosity and volume of minerals), using formation-specific parameters. The results were validated notably against the lithology observed in the mud logs. In GRT-1, the Jurassic and Triassic sedimentary section (Lias, Keuper, Muschelkalk and Buntsandstein) as well as the granite interval were interpreted; however, due to data availability, only the Buntsandstein could be interpreted for GRT-2.

2.2 Geological interpretation (borehole images)

Interpretation of ultrasonic and resistivity borehole image logs from GRT-1 and GRT-2 had been conducted prior to this study (Vidal et al., 2016; Dezayes et al., 2014; Hehn et al., 2016). However, a review of these logs was conducted to clearly distinguish the interpreted features (notably the fractures) in terms of their significance for the upcoming phases of the modelling. Drilling-induced features (tensile and shear fractures), which indicate the azimuth of the horizontal stress direction, were thus separated from natural fractures; and the latter were classified to distinguished resistive from conductive fractures, the latter being more likely to be open and therefore contribute to fluid flow. The output of this reinterpretation have been used for the fracture model (see Section 3).

2.3 Geomechanical interpretation

A wellbore mechanical earth model, or 1D MEM, is built first to define the mechanical properties, which are subsequently used for 3D mechanical modelling (section 7). Density and sonic logs (compressional and shear velocities), together with the results of the petrophysical interpretation, were combined to obtain the key mechanical properties along the GRT-1 well (static elastic moduli and rock strength parameters, such as compressive and tensile strengths as well as friction angle). Published correlations were selected for the computation, and the estimates were validated with values available in literature for the same formations in the nearby site of Soultz-sous-Forêts (Valley 2007; Cornet et al. 2007).

Subsequently, vertical stress was computed by extrapolating and integrating the bulk density log, and minimum and maximum horizontal stress were estimated with a poroelastic approach, incorporating assumptions on the regional tectonics (horizontal strains) and calibrating the resulting stress gradients against the observations made for Soultz (Cornet et al. 2007).

Finally, the geomechanical model was used to predict the occurrence of mechanical or hydraulic instability along the well trajectory. These results could be compared with the events observed in the well, such as the mechanical instabilities identified in the image and caliper logs (breakouts, tensile fractures, borehole shape) and the losses documented in the drilling reports. The results are displayed in Figure 2.1.

In the case of GRT-1, losses could not be predicted, as they are most likely to be ascribed to pre-existing fracture zones, as can be confirmed by the interpretation of petrophysical and image logs. On the other hand, a fair match of the breakout depths was obtained with the GRT-1 geomechanical model. It was also shown that tensile fractures can be predicted with good accuracy if thermal stresses are taken into account in the wellbore stability model. An accurate modelling of downhole temperatures and pressures, aiming at a more realistic estimate of thermal stresses, is currently ongoing and will be the subject of a separate publication.

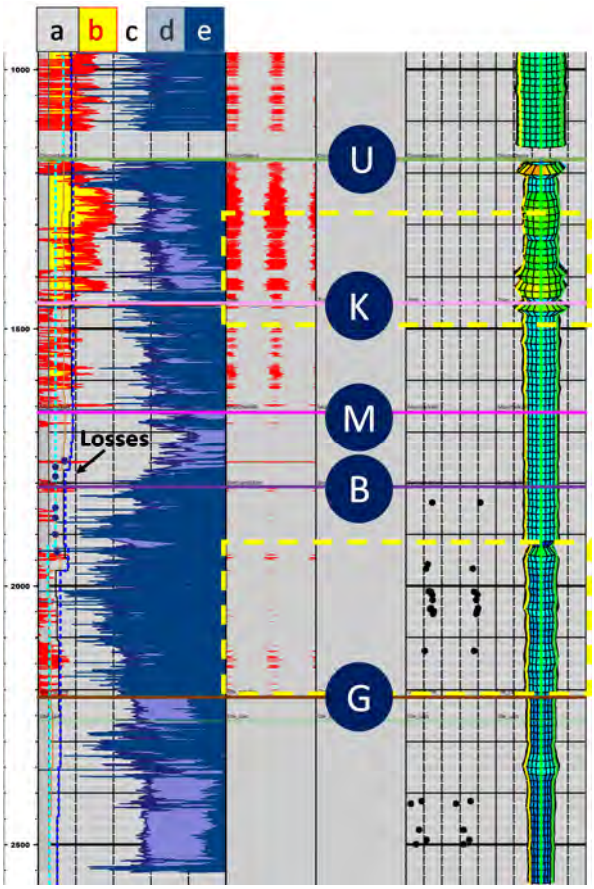

Figure 2.1: Post-drill wellbore stability analysis of well GRT-1 (1000 m MD – TD). Track 1: critical mud weights (a. kick, b. breakout, c. safe mud weight window, d. loss, e. breakdown; blue dots mark the observed losses); Track 2 and 3: synthetic failure image; Track 4: observed breakouts; Track 5: borehole shape. Corresponding synthetic and observed features are highlighted. Markers: U = Unconformity, K = top Keuper, M = top Muschelkalk, B = top Buntsandstein, G = top Granite.

The absence of the required input data in GRT-2 (notably sonic logs) made it impossible to repeat the workflow on that well. Therefore, it was decided to run a "blind test" by using the properties defined in GRT-1 to simulate a "pre-drill" stability model for GRT-2, and compare the results with the observed drilling events. The results (Figure 2.2) show that the pre-drill model would have predicted the occurrence of shear failure (breakouts) in the Lias formation with mud weights lower than 1.3 g/cc, and occurrence of tensile failure for mud weights higher than 1.9 g/cc. This formation was drilled with a mud weight between 1.07 and 1.12 g/cc, and indeed proved prone to mechanical instability, although clay swelling due to the long exposure of the formation to water-based mud probably worsened the situation. A pre-drill geomechanical analysis, therefore, may have allowed

to anticipate this behaviour and to adopt the most suitable mud weight, ultimately reducing the wellbore instability.

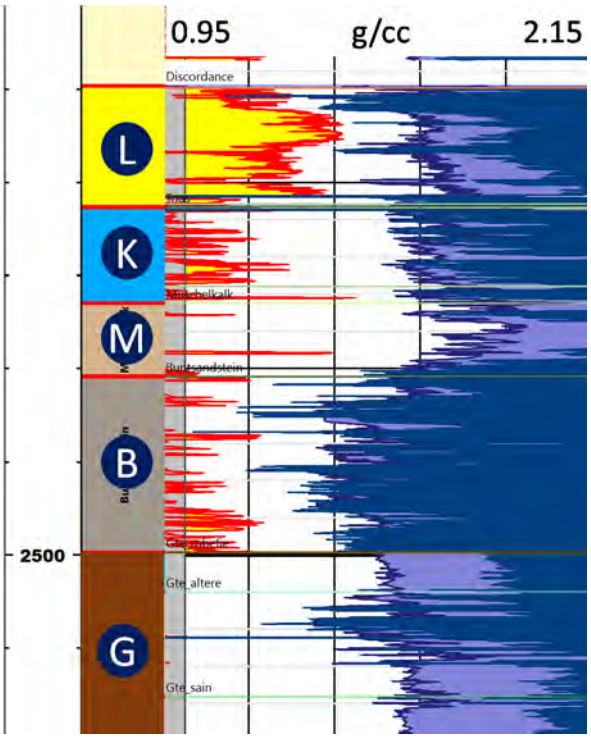

Figure 2.2: Pre-drill wellbore stability analysis of well GRT-2 (1000-3000 m MD). Track 1: zones (L = Lias, K = Keuper, M = Muschelkalk, B = Buntsandstein, G = Granite); track 2: critical mud weights (see Figure 2.1 for colour-coding).

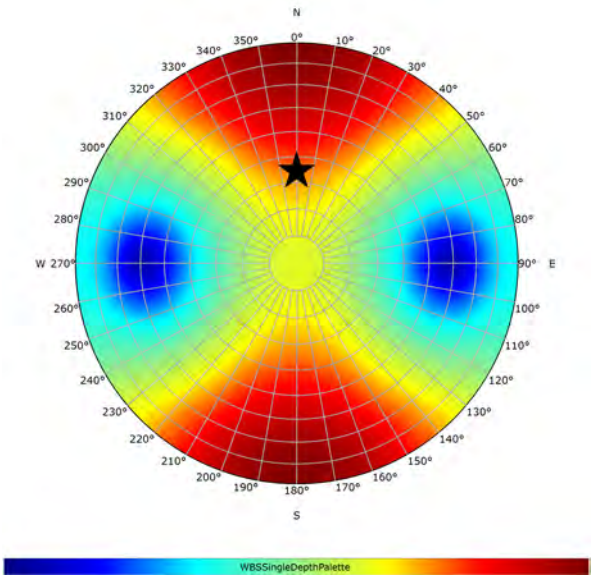

Figure 2.3: Sensitivity of critical breakout mud weight to borehole trajectory in GRT-2, Lias formation (1375 m MD). The star marks the actual azimuth and deviation. Colours range from more favourable conditions in blue (MW = 1.25 g/cc) to more critical in red (MW = 1.5 g/cc).

The sensitivity of the critical mud weights to the wellbore trajectory was evaluated at several depths within the Lias formation. The results show little dependency on wellbore deviation, but suggest that a more favourable azimuth may have slightly favoured the stability of GRT-2 (see Figure 2.3). This is due to the high stress disequilibrium, so that in a normal fault regime a trajectory aligned with the least horizontal stress direction (here, roughly E-W) would be less prone to mechanical instability.

3. GEOLOGICAL MODEL

As a next step in assessing the geomechanical impact of the geothermal activity, a geological model was built. The extent of the model is of 5x5 km around the two wells, as it was defined by the tests performed in order to identify the size of the drainage area of the wells.

The geological model consists in two main parts, the structural framework and the associated 3D grid.

3.1 Structural framework

The structural framework of the model was generated based on the available seismic interpretation.

The seismic interpretation (faults and main stratigraphic horizons) were provided by ES Geothermie. They were quality checked against the available 2D seismic lines and modified to include the major basal Tertiary unconformity (with a hiatus of 125 My).
All the seismic data were provided in time domain, therefore, once the structural framework was built, it needed to be depth converted. In order to depth convert, a velocity field was generated based on a layer cake strategy approach, using the seismic horizons and their corresponding depth well markers.

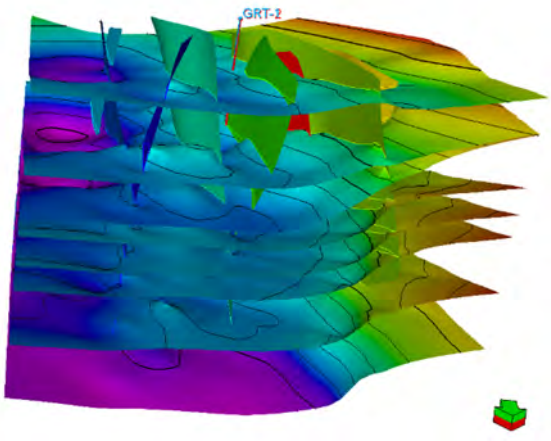

Figure 3.1: The structural framework. The model includes all the main stratigraphic horizons that delimit the main geological units (Schistes à Poissons from Rupelian, Unconformity, Top Trias, Top Muschelkalk, Top Buntsandstein and Top Granite).

3.2 3D grid

As soon as the structural framework was finalized and validated, the associated 3D grid was generated.

The 3D grid includes only the reservoir units (Muschelkalk, Buntsandstein and Granite). The seal and the overburden were not modelled in order to save computation time.
The horizontal resolution of the grid was set to 75x75 m, as for the vertical resolution, it varies from one geological unit to another, with of average of 22 meters, with a slightly lower value (19m) in the granite unit, which is considered to be the main flow unit. As a compromise, the grid resolution was defined in such a way to minimize computation time of the dynamic simulations (sections 6 and 7) as much as possible.

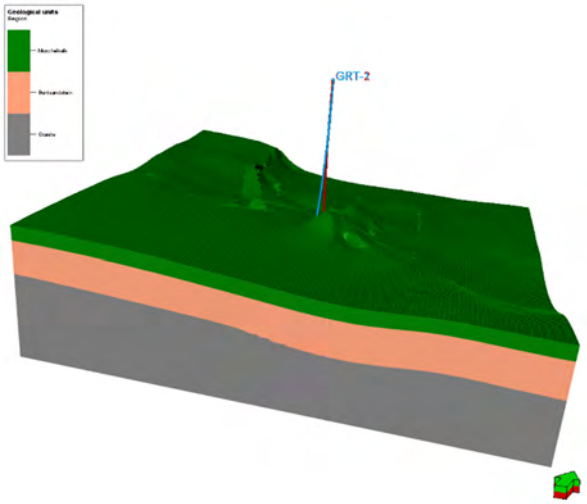

Figure 3.2: The grid contains 870000 cells.

4. FRACTURE MODEL

As mentioned previously, image logs were available for the sandstone layers in both wells but only in GRT-1 for the granite. The analysis of these images gave the distribution of natural fractures in the wells that was used to build the fracture model. To do so we have proceeded in three steps.

4.1 Fracture analysis

The first step to build a fracture model is to analyse the distribution of the fracture identified on the image logs. Figure 4.1 shows the stereonet view (lower hemisphere) of the poles (dots) of the fractures identified for GRT-1 (left) and GRT-2 (right), their strike distribution (as a rose diagram). On these plots, the discontinuities with a dip higher than 70° have been defined as joints (red dots) and those with a dip lower than 70° as faults/fractures (blue dots).

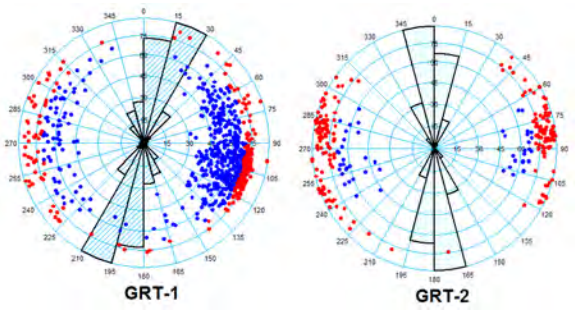

Figure 4.1: Distribution of the fractures in wells GRT-1 and GRT-2.

The analysis of these data shows that the fractures are mainly oriented N-S with a slight deviation to N20°E for GRT-1. From the figure it seems that there are more fractures in GRT-1 than in GRT-2, but the due to the deviation of the second well, the image log tool was not able to reach the granite layers, so only fractures in the Buntsandstein layer are visible for this well. From this analysis, P32 density logs (fracture area /volume) were computed for both wells and for each fracture types (joints and faults). These density logs will be used later on in the construction of the fracture network in section 3.3 below.

4.2 Natural Fracture Prediction

Before building the fracture network, it is important to identify the tectonic regimes associated with the fractures and joints identified in the wells. By this process, it will be deducted if there are one or several families of fractures (Legrand et al., 2013).

To do so, the faults in the structural framework of the model have been used, as well as the natural fractures identified in both wells.

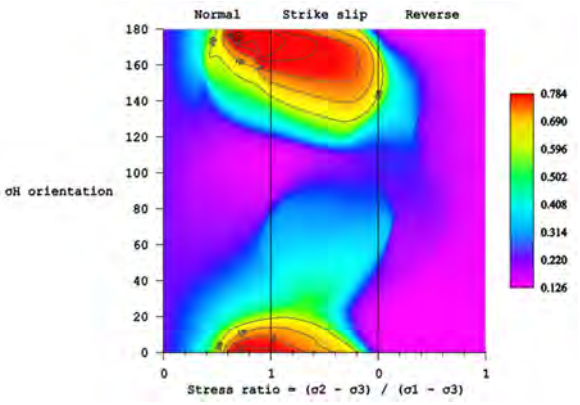

Figure 4.2: Tectonic regime resulting from the Natural Fracture Prediction process.

The resulting tectonic regime is a normal regime with a stress ratio of 0.784 (see Figure 4.2), which correspond to a strike-slip component to this normal regime (Angelier 1975). This is in agreement with the regional regime (Genter et al., 1995).

In the last part of this process it is possible to generate fracture drivers based on standardization method

which reproduces mean and standard deviation of observed well fracture density. These fracture drivers will be used to guide the computation of the fracture network as explained in the next section, such as orientation information (dip angle and dip azimuth) for both fracture types: joints and faults .

4.3 Fracture Network

To build the fracture network, it was first necessary to create a region in the grid corresponding to fault zones of 50 m away from each fault. In this fault zone region the density log from GRT-2 (which trajectory is very close to a fault) was upscaled with a distance to fault option so that the density of fractures is higher at the fault and lower 50m from it. For the rest of the grid the fracture density log from GRT-1 was used. To reduce the number of fracture patches in the model a hybrid fracture network was created, meaning a portion of it is modelled as Discrete Fracture Network (DFN) and another portion is modelled as Implicit Fracture Network (IFM). In the latter, the fractures are not modelled as objects but as a property in the grid.

The joints (here fractures with dip higher than 70° from the image log) were modelled as implicit network entirely. The fractures with dip lower than 70° from the image log were modelled as rectangular patches as both implicit and discrete networks. The ones with lengths larger that 200m were modelled as discrete and the ones with lengths smaller than 200m were modelled as implicit. The maximum length for these faults was set to 400m. To guide the orientation of the fractures, the fracture drivers parameters (dip angle and dip azimuth) that were computed in section 4.2 were used.

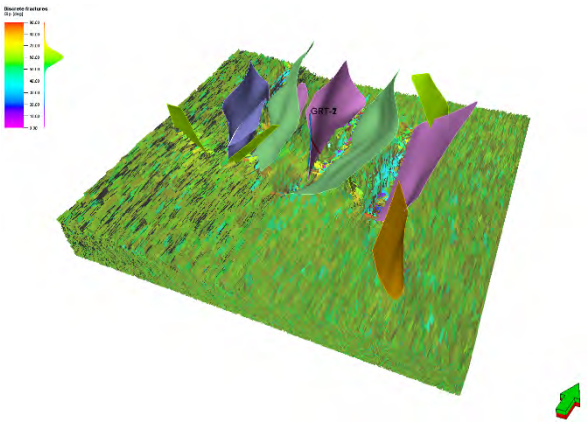

Figure 4.3: DFN resulting from the fracture modelling process.

Finally, default parameters for the aperture were chosen, as this information is quite difficult to obtain for the entire model. These defaults parameters are as follow; a log-normal distribution with maximum aperture at 3mm, mean aperture at 0.075mm and standard deviation at 0.0015mm. The DFN thus obtained is shown on Figure 4.3.

4.4 Upscaled Fracture Model

A property grid was generated based on the fracture model obtained. Both the discrete and implicit fracture networks were used, as well as the Oda method (Oda 1985) for the upscaling of the permeability property. The property obtained is shown on Figure 4.4 below.

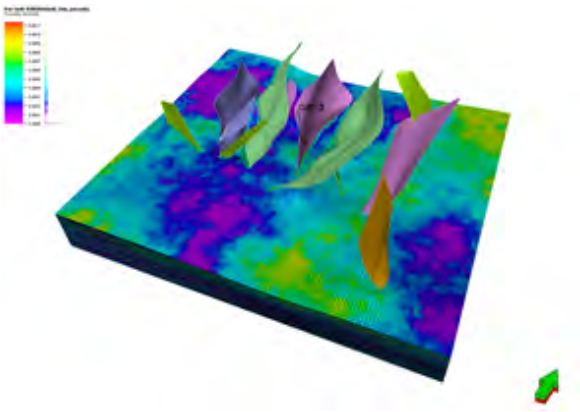

Figure 4.4: Property grid, here fracture porosity.

The mean fracture porosity obtained is 0.03% with a max at 0.1%. The mean permeability obtained ranges from 31mD in the X-direction to 171mD in the Z-direction.

5. SIMULTANEOUS SEISMIC INVERSION

The main objective of simultaneous seismic inversion consists in inverting seismic data into acoustic and elastic properties, using a linear approximation of the Zoeppritz equation. This task is done by building an "a priori" model that uses the well logs and horizons to fill the low-frequency gap of the seismic bandwidth. This low frequency model with 2D post-stack seismic lines and their associated wavelets are the inputs of the simultaneous inversion.

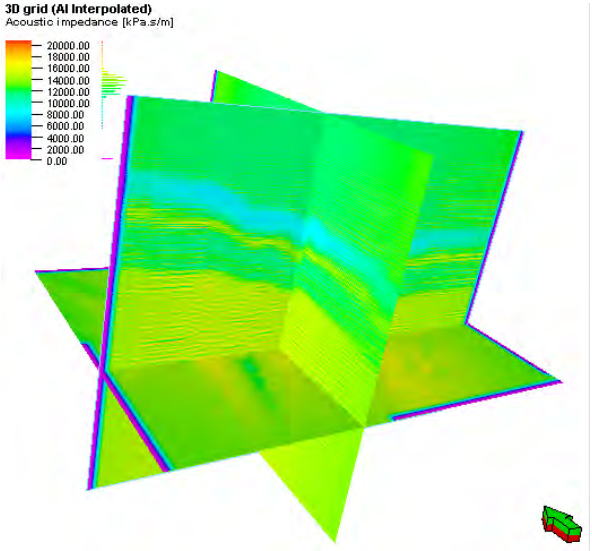

Figure 5.1: Acoustic impedance cube from inversion

The result of inversion is an estimation of the physical parameters across the prospect, both within and outside the well control. Since we used 2D post stack seismic lines, 2D acoustic impedance (AI) lines were generated and sampled in the model (figure 5.1), which was used as a trend in geomechanical property modelling.

6. DYNAMIC MODEL

Numerical simulation allows evaluation of many different scenarios under highly uncertain geological conditions. The creation of a dynamic model consists of two major steps: a) so called "history matching", where an attempt is made to reproduce measured pressures, temperatures and rates by modifying static reservoir parameters and boundary conditions, and b) different operational forecast scenarios. As a first step, matching of flow behaviour through the network system was de-coupled from stress analysis; full coupling is planned for a future update of the study.

6.1 Fluid Properties

According to the fluid analysis (Sanjuan et al. 2010, 2016b), total dissolved salt content of reservoir water was 100114ppm (100 g/l), resulting in a surface density of 1071.95 kg/m^3. Water was modelled as a single component, excluding the effect of free gas phase. Density variation with temperature was defined according (Sanjuan et al 2016b) with minimum density of 890 kg/m^3 at 200ºC.

6.2 History Matching: Initial Conditions

The first step in dynamic model setup was to correctly initialize the model by defining boundary conditions and build a temperature field model. Measured temperature logs in GRT-1 and GRT-2 were extrapolated using kriging algorithm with additional regional trends to keep the geothermal anomaly caused by the proximity of GRT-2 to the fault (white on Fig. 6.1). The temperature in GRT-2 at the same depth is higher by 14 ºC in comparison to GRT-1. This quick approach was used instead of natural state energy flow simulations, which are planned within the next phase, coupled with stress analysis.

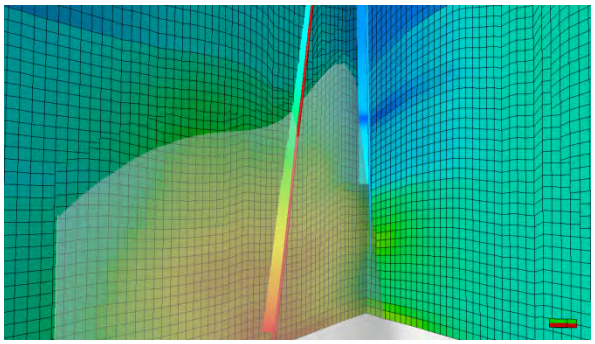

Figure 6.1: Temperature distribution after extrapolation (White surface represents the fault)

Simulation of fractured reservoir can be done with different approaches: a) explicit fracture modelling in single porosity concept, where the global or locally-refined cells are serving as highly conductive channels, b) Warren and Root approach, which uses homogenization of fracture properties in a dual porosity formulation (Warren at al., 1963). Previously it was shown that the main reservoir is associated with the fractured granite. Since the fluid flow and storativity are only associated with fractures and the heat concentrated in the non-permeable rock, we applied the Warren and Root method for single porosity formulation, with the assumption of homogeneous thermal properties (thermal rock conductivity and heat capacity). Dual porosity simulation will be only required in case when both heat and mass transfer present between permeable matrix and fracture system.

6.3 History Matching: Production and Tracer Tests

In 2013 the production tests in the GRT-1 well were followed by thermal and hydro-chemical stimulations. The second well from the duplet (GRT-2) showed better productivity in comparison to GRT-1. Following production tests in GRT-2 tracer test with injection of fluorescein and 2.7-napthalene disulphonate was carried at the end of 2014. During the tracer test about 60000 m^3 (average production rate 2470 m^3/day) were discharged from GRT-2 and 54000 m^3 (average injection rate 2130 m^3/day) re-injected back into GRT-1 (Sanjuan et al, 2016b).

History matching was performed in multiple stages first using measured rates, pressures and temperatures from each production test by applying multipliers on initial upscaled permeability values that were derived during step 4.4. The correction ranges from 2 to 20, depending on the permeability component. Results of the match are shown in the figure 6.2 showing good reproduction of measured values.

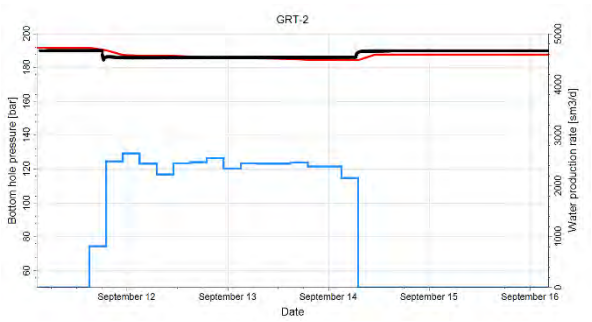

Figure 6.2: Example of history matched values for one of the production tests (blue line: observed and simulated water production rate; black line: observed BHP, red line: simulated BHP).

As a final step of history match the tracer test was simulated for the injection of 2.7-nds solution. Fluorescein was not used during history match because of relatively low reliability of the results.

In order to match the break-through time and observed concentrations further modification was needed to the permeability alongside the main fault. Results of the simulated versus observed produced tracer concentrations are shown on the figure 6.3.

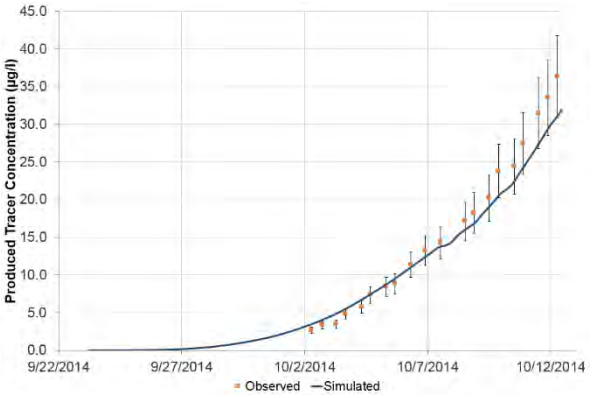

Figure 6.3: Simulated versus observed produced tracer concentration.

6.4 Development Forecast

Development of the geothermal system was simulated with the assumption of closed system (no fluid losses). Prediction is done for 50 years of operation with flow rates 100 m^3/h (2400 m^3/day). Cold water was re-injected into the reservoir at 70 ºC and average bottom-hole pressure of 191 bars. As we can see from the plots on the figure 6.4 production temperature slightly decreased due to insignificant cooling of the system that also resulted in a slight increase of the bottom-hole pressure of GRT-2.

Propagation of cooling front is dominant in the direction of the main fault and general fracture network. After 50 years the volume of rock cooled down by re-injection of 43.8 MM m^3 water is 60MM m^3. Cool front advanced for 700 m away from injection well GRT-1 (Figure 6.5).

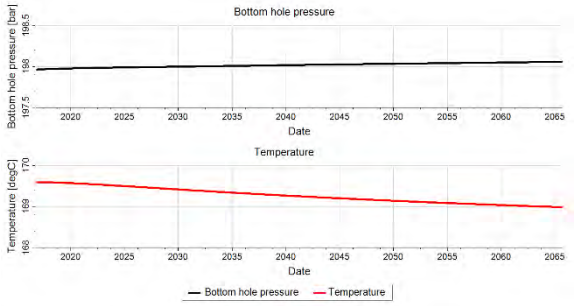

Figure 6.4: Forecasted simulated temperatures and bottom hole pressure for GRT-2 at constant production rate of 2400 m^3/d.

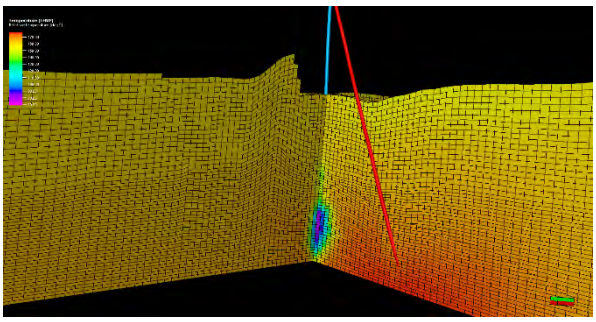

Fig. 6.5: Reservoir cooling after 50 years.

7. 3D GEOMECHANICAL MODEL

The reservoir is mechanically coupled to the surrounding rock masses, therefore, the surrounding rock masses most be included when studying the deformation of the reservoir due to production or, in this case, geothermal activities. Thus, the geomechanical model will include, apart from the reservoir model, the surrounding formations (over-, under- and side-burdens).
Building a geomechanical model also requires applying boundary conditions as well as defining the mechanical properties of the intact rocks, fractures and faults.

7.1 Description of the geomechanical model

The first step in building the geomechanical model is to embed the reservoir by adding the overburden, all the way to ground level, and underburden formations.
The overburden was defined using as input the main stratigraphic horizons defined in the structural framework. As for the upper most surface, it was generated based on the ground level values of the surrounding wells.

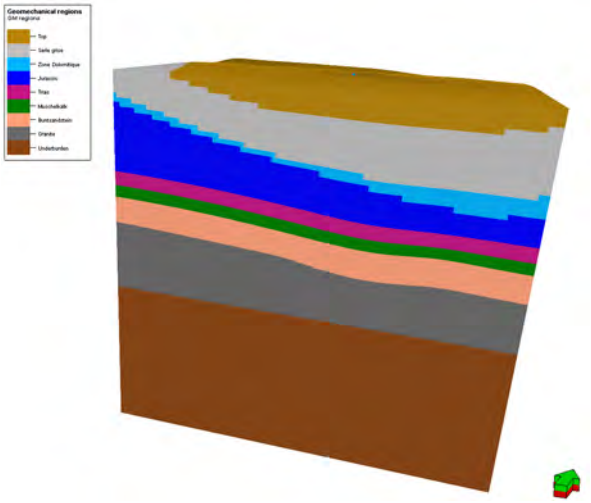

Fig. 7.1 Geomechanical grid; apart from the simulation grid, over- and under-burden were added. The grid contains 1.7 million cells.

7.2 Geomechanical properties

In order to define the key mechanical properties of the intact rocks (elastic properties and rock strength as well as the friction) the corresponding properties estimated during the wellbore data analysis stage *(*see section 2.3) were used.
The mechanical properties derived along the GRT-1 well were upscaled into the geomechanical model and extrapolated to populate the entire model, using the Kriging algorithm. In order to account for the lateral variability of the properties, a seismic inversion was performed (see section 5) and the resulted Acoustic Impedance property was used as a regional trend.

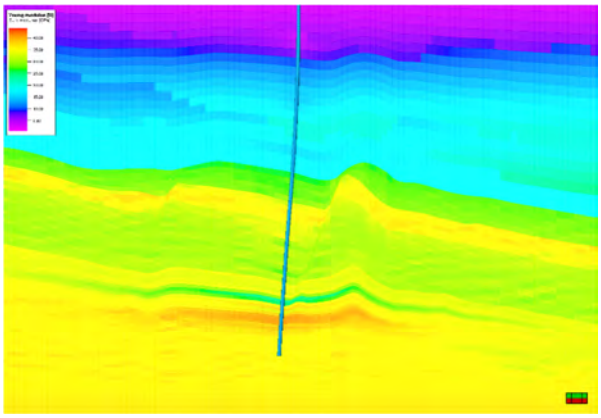

Fig. 7.2 Young Modulus property, E-W vertical cross section through the GRT-1 well

There was no information regarding the fault/DFN mechanical parameters, therefore they were calculated based on the intact rock's mean Young's modulus.

7.3 Boundary conditions

Once the mechanical properties are defined for both intact rocks and discontinuities, boundary conditions (regional stresses) needed to be applied at the limits of the model to calculate the initial stress state.
For this study, the regional stress were generated by applying displacement boundary conditions. The displacements used were defined during the geomechanical interpretation in the GRT-1 well (notably in the poroelastic stress modeling, by deriving the tectonic strains that correspond to the expected stress regime and gradients; see section 2.3).
The orientation of the Maximum horizontal stress was set to N0°E to be in agreement with the observations made during the fracture analysis along the two wellbores.

7.4 Geomechanical simulation

In order to calculate the initial stress state as well as the changes due to the geothermal activity, a finite-element simulator was used.

The simulation run was split in two steps. Firstly, an initialisation step was performed to reach the mechanical equilibrium between the applied boundary conditions and the initial state of stress in the model.
This step allowed the calibration of the geomechanical grid (mechanical properties and boundary conditions) by comparing the simulated and the calculated stresses along the GRT-1 trajectory and modifying the parameters until a good match was achieved.
The figure 6.3 shows the comparison between the simulated principal stresses and the calculated ones along the GRT-1 well trajectory.
After the model was validated and the initial stress conditions were calculated, a partially coupled simulation run was performed, including the pressures and temperatures calculated during the History Matching and Forecasting processes, in order to assess the impact the geothermal activities on the existing discontinuities and the adjacent formations.

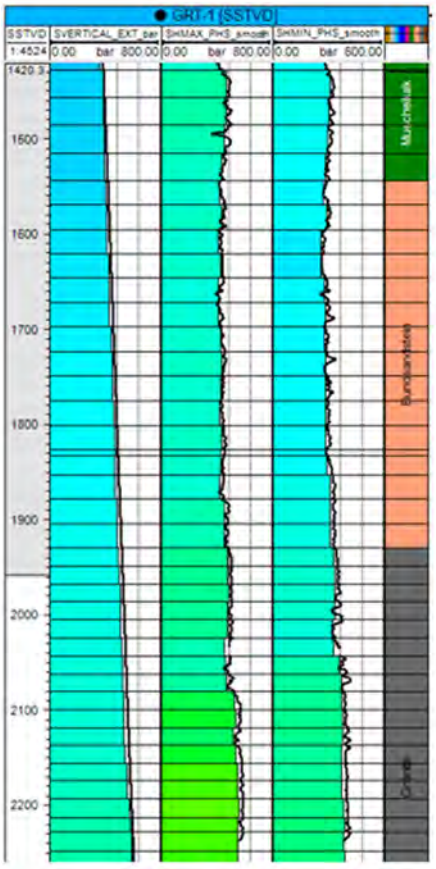

Fig. 7.3: Cross section along the GRT-1 trajectory; from left to right both simulated (colored) and calculated (black line) principal stresses: Sv, Shmax and Shmin.

Analysing the results it was observed that the cooling of the rock around the injection well (GRT-1) causes changes in the in-situ stresses.

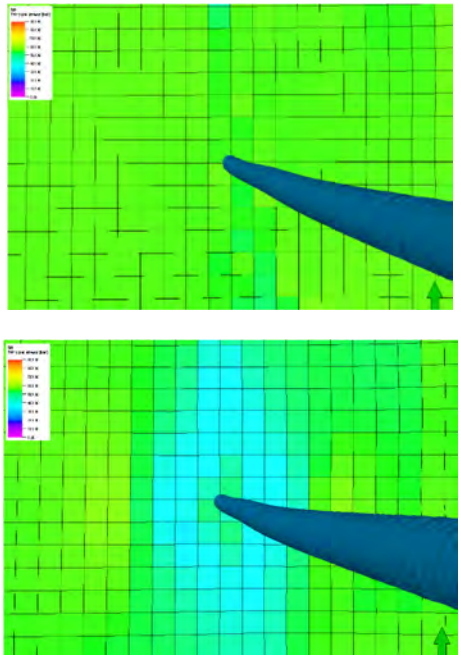

Fig. 7.4: Principal horizontal stress (Shmax) around the GRT-1 well at Time=0 (left) and Time=50 years (right); horizontal cross section at 2300 m depth, in the granite unit.

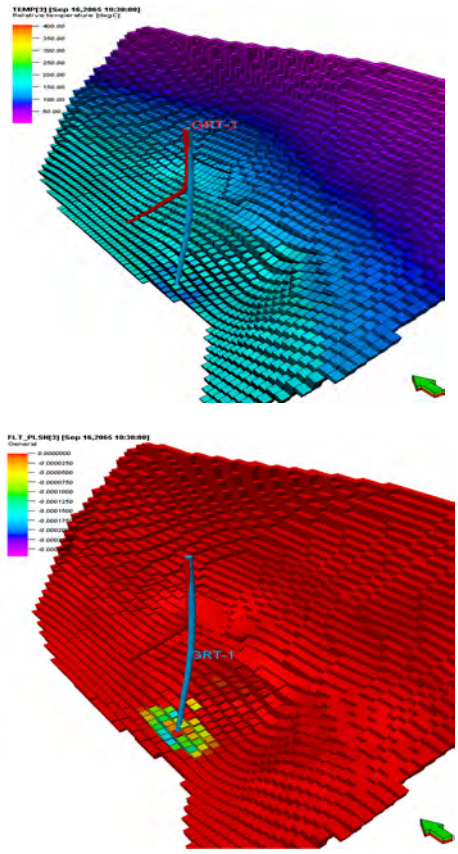

Fig. 7.5: Temperature (left), Fault Shear Strain (right) properties that were calculated after 50 years of geothermal operations, are displayed along the fault near the two wells.

Consequently, strain accumulations were identified on the main fault and fractured zone near the two wells, as observed in Fig. 7.5, the strains are localized mainly around the GRT-1 well, in the vicinity of the fault. The presence of strain, especially shear strain, leads to the conclusion that a mobilisation of fractures and fault segment situated in the cooling area of GRT-1 may occur.
A sensitivity study on various geomechanical parameters (e.g. fault/DFN geomechanical and thermal behaviour, boundary conditions) is currently carried out in order to validate these results.

8. CONCLUSIONS

An integrated model combining the geological characteristics, fluid and heat flow, and geomechanical behaviour was built for the site of the Rittershoffen geothermal power plant. A multi-disciplinary team analysed and interpreted the input data from the GRT-1 and GRT-2 well and from the available seismic surveys.

The wellbore-centric geomechanical modelling of GRT-1 was validated against offset data (notably for Soultz) and calibrated by matching the observed drilling-induced events. The application of this model to GRT-2 showed that some of the mechanical instabilities observed in the second well could have been predicted by geomechanical modelling. Advanced pressure and temperature modelling is ongoing to improve the accuracy of the wellbore stability analysis.

Based on the fractures observed in the two boreholes and on the major faults, the tectonic events causing the occurrence of fractures in the Buntsandstein could be identified and used to model the distribution and orientation of the natural fractures in 3D. The results were used to derive a permeability model for dynamic simulations.

The inversion of 2D seismic lines resulted in a laterally continuous model of acoustic amplitude, which provided precious information on the variability of reservoir properties away from the wells.

The dynamic model (fluid and heat flow) was validated by matching the production and tracer tests conducted in the wells. Based on this model, it was possible to forecast the pressure and temperature changes induced in the surrounding of the well in 50 years of operations of the site.

The 3D geomechanical model was based on the wellbore mechanical model, extrapolated with the support of seismic inversion, and incorporating the natural fracture network. By coupling it to the flow and heat model, the impact of pressure changes and thermal stresses could be observed.

The impact of stress changes on fracture permeability can be modelled by the iterative coupling of the flow and mechanical model. Moreover, shear stress in

correspondence of discontinuities, such as faults and fractures, may cause their reactivation, which in turn could generate micro-seismic events. Two-way coupling of the models, as well as the analysis of the fault and fracture stability and the prediction of the location and magnitude of microseismic events, are currently being carried out.

The execution of this multi-disciplinary workflow in an integrated software environment has facilitated the collaboration and ensured more consistency between the different domains.

REFERENCES

Angelier, J., Sur l'analyse de mesures recueillies dans des sites faillés: L'utilité d'une confrontation entre les méthodes dynamiques et cinématiques, *Compte Rendu de l'Académie des Sciences*, Paris, (D) **281,** (1975), 1805-1808.

Baujard, C., Genter, A., Graff, J.-J., Maurer, V., and Dalmais, E.: ECOGI, a New Deep EGS Project in Alsace, Rhine Graben, France, *Proceedings World Geothermal Congress 2015*, Melbourne, Australia, (2015), paper #001, 19-25.

Cornet, F.H., Bérard, Th., Bourouis. S., How close to failure is a granite rock mass at a 5km depth? *International Journal of Rock Mechanics & Mining Sciences* **44** (2007), 47–66.

Dezayes, Ch., Sanjuan, B., Gal, F., Lerouge, C., Fluid geochemistry monitoring and fractured zones characterization in the GRT1 borehole (ECOGI project, Rittershoffen, Alsace, France), in: Proceedings of Deep Geothermal Days. Paris, France (2014).

Genter, A, Traineau, H., Dezayes, Ch., Elsass, Ph., Ledesert, B., Meunier, A., Villemin, Th., Fracture analysis and reservoir characterization of the granitic basement in the HDR Soultz Project (France), *Geothermal Science and Technology* **4**(3) (1995), 189-214.

Genter, A., Vidal, J., Baujard, C., Dalmais, E., Schmittbuhl, J., Permeability in deep-seated granitic rocks: lessons learnt from deep geothermal boreholes in the Upper Rhine Graben, *20th International Association of Hydrogeologists*, 09-10 June 2015, La Roche-sur-Yon, France (2015).

Hehn, R., Genter, A., Vidal, J., Baujard, C., Stress field rotation in the EGS well GRT-1 (Rittershoffen, France). European Geothermal Conference 2016, EGC2016, 19-22 September 2016, Strasbourg, France (2016).

Legrand, X., Joonekindt, J. P., Lee, B. C., LeFranc, M., Maerten, L., Anis, L., Innovative natural fracture prediction using geomechanically-based solution: application to the Malay Basin (Malaysia). 2nd EAGE Workshop, 8-11 December, 2013, Muscat, Oman.

Longuemare, P. et al., Geomechanics in Reservoir Simulation: Overview of Coupling Methods and Field Case study, *Oil & Gas Science and Technology – Rev. IFP,* **57** (2002), No. 5, 471-483

Oda, M., Permeability tensor for discontinuous rock masses, *Geotechnique*, **35**, (1985), 483–495.

Sanjuan, B. , Millot, R., Dezayes, C., Brach, M. Main characteristics of the deep geothermal brine (5 km) at Soultz-sous-Forets (France) determined using geochemical and tracer test data. C. R. Geoscience 342, (2010), pp. 546–559.

Sanjuan, B., Millot, R., Innocent, Ch., Dezayes, Ch., Scheiber, J., Brach, M. Major geochemical characteristics of geothermal brines from the Upper Rhine Graben granitic basement with constraints on temperature and circulation, Chemical Geology, 428 (2016a), pp.27-47.

Sanjuan, B., Scheiber, J., Gal, F., Touzelet, S., Genter, A., Villadangos, G., Interwell chemical tracer testing at the Rittershoffen site (Alsace, France). European Geothermal Conference 2016, EGC2016, 19-22 September 2016, Strasbourg, France (2016b).

Valley, B. The relation between natural fracturing and stress heterogeneities in deep-seated crystalline rocks at Soultz-sous-Forêts (France), PhD thesis, ETH Zurich, Switzerland, 260 pp. (2007).

Vidal, J., Chopin, F., Genter, A., Dalmais, E., Natural fractures and permeability at the geothermal site Rittershoffen, France. European Geothermal Conference 2016, EGC2016, 19-22 September 2016, Strasbourg, France (2016).

Warren, J.E.. Root, P.J. The bevavior of naturally fractured reservoirs crystalline rocks at Soultz-sous-Forêts (France), PhD thesis, ETH Zurich, Switzerland, 260 pp. (2007).

Acknowledgements

The authors would like to thank ES Géothermie for sharing their data for this study. Special thanks to Marta Krasinska-Cwyl, Claudia Sorgi, Jean Pierre Joonnekindt and Marie LeFranc at Schlumberger, as well as to Régis Hehn at ES Géothermie, for their contribution to this project. The work has been done on Schlumberger software (Petrel™, Techlog™, VISAGE™, ECLIPSE™).